Regional Stress Orientations and Slip Compatibility of Earthquake Focal Planes in the New Madrid Seismic Zone

by Owen Hurd and Mark D. Zoback

INTRODUCTION

The New Madrid seismic zone (NMSZ) in the central United States is one of the most active regions of intraplate seismicity in North America and site of the devastating 1811–1812 earthquake sequence (Nuttli, 1973; Johnston and Schweig, 1996). The NMSZ lies within the NE–SW trending Reelfoot rift (Fig. 1), which represents a failed rift arm that developed during the Late Proterozoic and Early Cambrian opening of the Iapetus Ocean on the southeast margin of early North America (Ervin and McGinnis, 1975). Fault offsets inferred from seismic reflection and trench data suggest that current seismicity levels likely initiated during the Holocene (Pratt, 1994; Schweig and Ellis, 1994; Van Arsdale, 2000) when optimally-oriented Proterozoic and Cambrian faults were reactivated in the contemporary stress field (Zoback *et al.*, 1980; Braile *et al.*, 1986; Dart and Swolfs, 1998). The recurrence of large and potentially damaging earthquakes in late Holocene time (Tuttle *et al.*, 2005) may be a response to Pleistocene deglaciation (Grollimund and Zoback, 2001; Calais *et al.*, 2010).

Contemporary seismicity illuminates a complex network of fault trends and deformation styles within the NMSZ (Stauder *et al.*, 1976; Andrews *et al.*, 1985; Himes *et al.*, 1988; Chiu *et al.*, 1992; Liu, 1997; Pujol *et al.*, 1997; Mueller and Pujol, 2001; Dunn *et al.*, 2010), although the seismic zone is characterized by three primary faults; the southern, NE-striking Axial fault, the central, NNW-striking Reelfoot fault, and the northern, NE-striking New Madrid North fault (Johnston and Schweig, 1996; Baldwin *et al.*, 2005; Csontos and Van Arsdale, 2008). The Axial and New Madrid North faults exhibit strike-slip motion on near-vertical fault planes while thrust motion characterizes the southwest-dipping Reelfoot fault (Liu, 1997; Saint Louis University Earthquake Center). The fault patterns and senses of offset, which have been interpreted as a dextral strike-slip fault system with a left-stepping crossover (Russ, 1982), are geometrically consistent with those expected for active faults in an ENE-WSW compressive stress field (Zoback and Zoback, 1981). What remains to be examined in detail, however, is whether or not the faults and senses of offset are frictionally consistent with slip in the current stress field.

In this paper, we investigate whether or not local stress sources or anomalous fault strengths are required to explain active NMSZ faulting. Twelve well-constrained individual earthquake focal plane mechanisms augment previously available stress information and allow us to examine the frictional consistency of NMSZ fault planes. Following the methodology described in Zoback (1992), the new focal plane mechanisms are used to update the regional stress map, evaluate the consistency of maximum horizontal compressive stress ($S_{H\max}$) orientations, and investigate fault stability using the Mohr–Coulomb failure criterion.

DATA COLLECTION

Since we use earthquake focal mechanisms to infer stress orientations and calculate relative stress magnitudes, it is crucial that the selected mechanisms are well constrained. To ensure sufficient quality, all focal mechanisms are from **M** >2.5 earthquakes and are constrained by waveform modeling. This modeling technique commonly uses relative body-wave amplitudes combined with a broader search range over the focal sphere to constrain solutions, and often provides more reliable focal mechanisms than those derived solely from *P*-wave first-motion polarities (Lay and Wallace, 1995).

Twelve new focal mechanisms are compiled that do not overlap with the Zoback (1992) dataset. Ten mechanisms are from the Saint Louis University Earthquake Center North America Moment Tensor Catalog or the Lamont-Doherty Cooperative Seismograph Network Catalog (Table 1). The remaining two focal mechanisms were originally published in Herrmann (1979) and were designated slip-incompatible in the current stress field by Zoback (1992). However, Herrmann and Ammon (1997) revised the two focal mechanisms using improved waveform modeling techniques, and we reexamine both updated mechanisms in this study.

To examine slip compatibility of NMSZ faults, we utilize the individual focal mechanism nodal planes as well as large-scale fault planes delineated from hypocenter distributions

 doi: 10.1785/0220110122

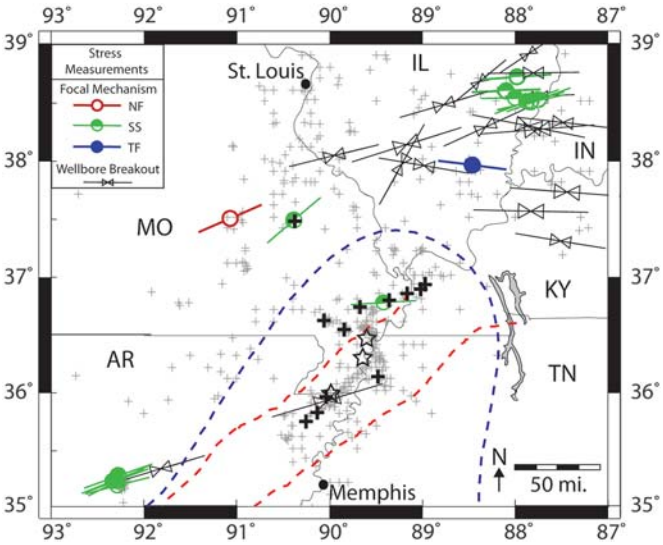

▲ **Figure 1.** Major tectonic structures, seismicity and stress measurements in the New Madrid seismic zone. The black crosses represent the 12 earthquakes examined in this study while the black stars represent approximate locations of the three mainshocks in the 1811–1812 earthquake sequence (Tuttle *et al.*, 2005). Other earthquakes (gray crosses) are from the USGS/NEIC catalog (1973–2010). Stress measurements are from the 2008 World Stress Map database and the Saint Louis University Earthquake Center (NF = normal faulting, SS = strike-slip faulting, TF = thrust faulting). Bars on focal mechanisms and wellbore breakouts indicate the orientation of $S_{H\max}$. Red and blue dashed lines indicate boundaries of the Reelfoot rift and Mississippi embayment, respectively (after Csontos and Van Arsdale, 2008).

within the NMSZ. Specifically, we consider fault geometries representing the New Madrid North, Reelfoot (northern and southern segments), and Axial faults (Table 2) (Csontos and Van Arsdale, 2008).

UPDATING STRESS ORIENTATIONS

Using the 12 new focal mechanism *P*-axes, we first update the stress map in the New Madrid seismic zone and evaluate the consistency of $S_{H\max}$ orientations. Although a *P*-axis may deviate substantially from the maximum principal stress orientation in the absence of friction (McKenzie, 1969), experience has shown that *P*-axes in intraplate regions are consistent with maximum principal stress orientations from other stress indicators (Zoback and Zoback, 1980). The average *P*-axis trend of the 12 focal mechanisms is N84°E ± 7.4°. This ENE-WSW trend is consistent with nearby stress measurements in the 2008 World Stress Map (WSM) database from a variety of different stress indicators (Heidbach *et al.*, 2008) (Fig. 1). In particular, we note the consistency with $S_{H\max}$ orientations inferred from borehole breakouts within regions of active faulting in northeastern Arkansas. The ENE-WSW trend represents a slight, clockwise rotation from the NE–SW $S_{H\max}$ orientation found throughout much of central and eastern North America (Zoback and Zoback, 1980).

CONSTRAINTS ON RELATIVE PRINCIPAL STRESS MAGNITUDES

To evaluate slip compatibility on New Madrid fault planes, we follow the approach in Zoback (1992) to calculate relative principal stress magnitudes from the focal mechanism nodal planes and the local stress tensor geometry using independent stress observations. The stress tensor geometry near each earthquake is estimated by calculating the average $S_{H\max}$ orientation of the three nearest A- or B-quality stress measurements in the WSM database (see Zoback and Zoback [1989] for details on the quality ranking system). In the NMSZ, all of the A- and B-quality stress measurements are from borehole breakouts. Thus, $S_{H\max}$ is inferred independent of focal mechanism data. For each of the 12 $S_{H\max}$ estimates, the standard deviation about the mean is less than 15°. The remaining principal stress orientations are constrained assuming that the three principal stresses lie perpendicular to one another in vertical and horizontal planes (Zoback and Zoback, 1980). In this area, this assumption is validated by the NMSZ stress inversion in Mazzotti and Townend (2010) that illustrates nearly vertical and horizontal principal stresses.

The relative principal stress magnitudes are constrained with two physical relationships. The first relationship limits the allowable orientation of nodal plane slip vectors in the current stress field as defined by the magnitude of the intermediate principal stress (Angelier, 1979):

$$\Phi = \frac{S_2 - S_3}{S_1 - S_3} \tag{1}$$

S_1, S_2, and S_3 represent the three principal stresses in order of decreasing magnitude. Thus, Φ must fall between zero and one. Physically, this indicates that slip in the direction of the nodal plane slip vector is possible within the given stress configuration. Following Gephart (1985), Φ is calculated from the geometries of the two focal mechanism nodal planes and the three principal stresses:

$$\Phi = \frac{\beta_{13}\beta_{23}}{\beta_{12}\beta_{22}} + 1 = \frac{\beta_{33}\beta_{23}}{\beta_{32}\beta_{22}} + 1 \tag{2}$$

β_{ij} corresponds to a matrix of angle cosines relating the principal stress and focal mechanism coordinate systems. Note that (2) yields a Φ value for both nodal planes, and therefore identifies which of the two nodal planes, if either, is geometrically consistent with slip in the current stress field (satisfies $0 \le \Phi \le 1$). For each of the 12 focal mechanisms, we find that only one of the two nodal planes is geometrically consistent. We will examine the frictional slip consistency of the nodal planes in the next stage of the analysis.

Table 1
New and Revised Focal Plane Mechanisms Compiled for this Study

Date yyyy/mm/dd	Lat (°N)	Long (°W)	Z (km)	M_w	Strike (°)	Dip (°)	Rake (°)	Type	S_H Azi (°N E)	Φ	Δstr (°)	Δdip (°)	Ref
1963/03/03	36.64	90.05	15	4.7	304	78	−28	SS	83	0.727	3	2	1
					40	**63**	**15**						
1967/07/21	37.44	90.44	15	4.0	350	60	135	T	82	0.309	3	2	1
					116	**52**	**40**						
1991/05/04	36.56	89.83	8	4.1	**90**	**67**	**20**	T	83	0.087	16	10	1
					352	72	158						
1996/11/29	35.97	90	11	3.8	**120**	**65**	**15**	T	75	0.196	4	1	2
					24	76	164						
2003/06/06	36.89	89.01	0.5	4.0	250	80	155	SS	96	0.71	21	2	3
					345	**65**	**11**						
2004/06/15	36.73	89.68	4.5	3.5	175	55	70	T	83	0.363	2	9	2
					27	**40**	**116**						
2004/07/16	36.86	89.17	4	3.5	43	71	159	SS	88	0.099	2	12	2
					140	**70**	**20**						
2005/02/10	35.75	90.23	14	4.1	**55**	**80**	**−165**	SS	75	0.589	7	4	2
					322	76	170						
2005/05/01	35.83	90.15	8	4.2	**315**	**60**	**20**	SS	75	0.447	9	4	2
					214	74	148						
2005/06/02	36.14	89.46	15	3.9	**155**	**65**	**70**	T	88	0.574	5	18	2
					18	32	128						
2005/06/20	36.95	88.96	9	3.7	315	80	10	SS	96	0.086	0	20	2
					223	**81**	**179**						
2010/03/02	36.79	89.36	5	3.4	211	86	135	SS	83	0.378	4	1	2
					305	**45**	**5**						

The preferred nodal plane is indicated in bold. Δstr and Δdip are strike and dip misfits (in degrees) between the preferred nodal plane and the nearest test plane that slips with $\mu = 0.6$. SS = strike – slip, T = thrust. References: (1) Herrmann and Ammon (1997); (2) Saint Louis University Earthquake Center; (3) Lamont-Doherty Cooperative Seismograph Network.

The second physical relationship constrains relative principal stress magnitudes based on the frictional strength of optimally-oriented faults in the crust:

$$\frac{S_1 - P_P}{S_3 - P_P} = [(\mu^2 + 1)^{1/2} + \mu]^2 \tag{3}$$

P_P is the pore pressure and μ is the coefficient of fault friction (Jaeger and Cook, 1979). For given values of P_P and μ, the differential stress magnitudes cannot exceed the stress required to cause shear failure on preexisting, optimally-oriented faults in the brittle crust. Therefore, (3) provides an upper bound on the ratio of the maximum and minimum effective stresses. The relative principal stress magnitudes are calculated using (1), (2), and (3) assuming hydrostatic P_P in the brittle crust (Zoback and Townend, 2001), $\mu = 0.8$ (Byerlee, 1978), and $S_V = 25$ MPa/km (overburden density = 2,500 kg/m^3).

SLIP COMPATIBILITY

The final analysis step uses three separate approaches to examine the frictional slip compatibility of NMSZ fault planes in the contemporary stress field using the Mohr–Coulomb failure criterion. The Mohr–Coulomb criterion for slip on a preexisting, cohesionless fault is given by:

$$\tau = \mu(S_N - P_P) \tag{4}$$

τ and S_N are the shear and normal stresses acting on the fault plane, respectively. Slip occurs when the shear stress exceeds the frictional strength of a fault and the effective normal stress acting on a fault. The slip compatibility analysis will quantitatively determine the friction coefficients required for shear failure on NMSZ fault planes.

In the first approach, we begin by calculating the relative principal stress magnitudes near each earthquake. Because the magnitudes are calculated directly from the nodal plane and

Table 2
New Madrid Fault Planes Examined for Frictional Slip Compatibility

Strike (N°E)	Dip (°)	μ	Description
46	90	0.7562	Axial fault (AF)
29	72	0.5879	New Madrid North fault (NMNF)
167	30	0.7858	Reelfoot fault, northern segment (RFN)
150	44	0.68	Reelfoot fault, southern segment (RFS)

The friction coefficient (μ) required for Coulomb failure on the fault plane considers a uniform, transpressional stress field with hydrostatic pore pressure. All fault plane orientations are from Csontos and Van Arsdale (2008)

local $S_{H\max}$ orientations, they vary from earthquake to earthquake. Next, a set of test planes are created for each focal mechanism by perturbing the nodal plane strikes and dips up to ±45° in 1° increments. For each test plane, we then compute the friction coefficient required for failure using the Mohr–Coulomb criterion assuming hydrostatic pore pressure. The results of a friction coefficient calculation for a thrust and strike-slip focal mechanism are shown in Figure 2a and b, respectively. The strike and dip of the actual focal mechanism nodal planes are denoted by black dots. Test plane configurations where slip is frictionally impossible in the current stress field are indicated by hatched areas. All 12 focal mechanisms have one nodal plane on which shear slip is frictionally possible. That is, for one of the two nodal planes, the black dot falls within a colored region. We denote this nodal plane as the preferred nodal plane for each focal mechanism (Table 1). All preferred nodal planes were also geometrically consistent with slip ($0 \le \Phi \le 1$).

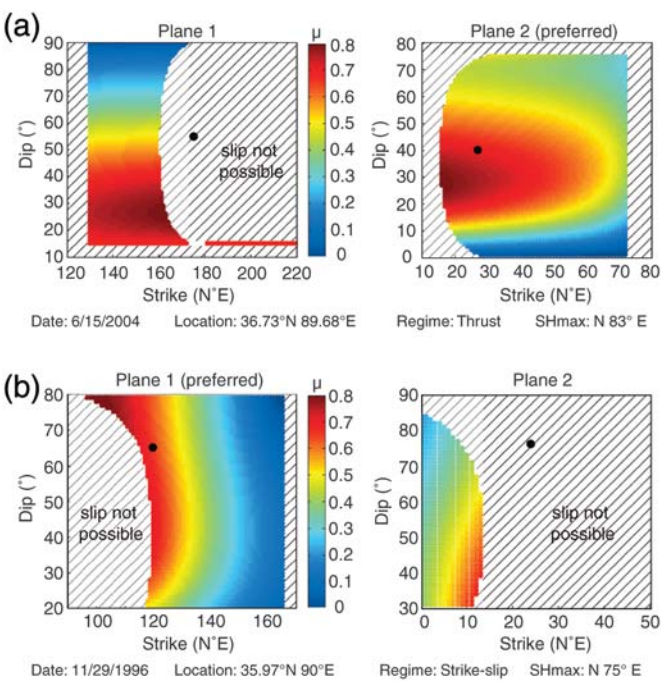

▲ **Figure 2.** Frictional slip compatibility results for a thrust (a) and strike-slip (b) focal mechanism analyzed in this study. Focal mechanism nodal plane orientations are indicated by black dots. The friction coefficients (μ) required for Coulomb failure on the test planes in the local stress field are scaled by color. Test plane configurations where slip is frictionally impossible in the local stress field are indicated by hatched areas. Only one nodal plane from each focal mechanism is frictionally consistent with slip in the local stress field (black dot falls within a colored region) and is identified as the preferred nodal plane.

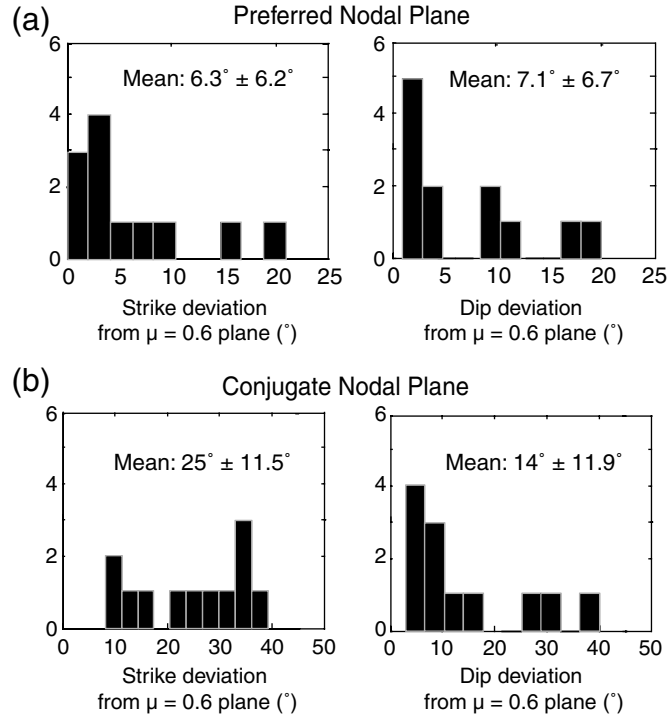

▲ **Figure 3.** Histograms displaying the misfit in strike and dip between the preferred (a) and the conjugate (b) focal mechanism nodal planes and the nearest well-oriented test plane that slips with $\mu = 0.6$ in the local stress field. The preferred nodal planes deviate on average less than 8° in strike and dip from the nearest well-oriented test plane. Note the different scales between preferred and conjugate nodal plane histograms.

For each focal mechanism, we then select the test planes that would slip with $\mu = 0.8$ and $\mu = 0.6$ which are most similar in orientation to the focal mechanism nodal planes. These test planes are identified as well oriented for failure in the current stress field. Next, we calculate the misfit in strike and dip between the well-oriented test planes and each of the focal mechanism nodal planes. Histograms of the misfits for the preferred and conjugate nodal planes for all 12 earthquakes are shown in Figure 3a and b, respectively. The preferred nodal plane deviates on average only ~6° in strike and ~7° in dip from the nearest well-oriented test plane that slips

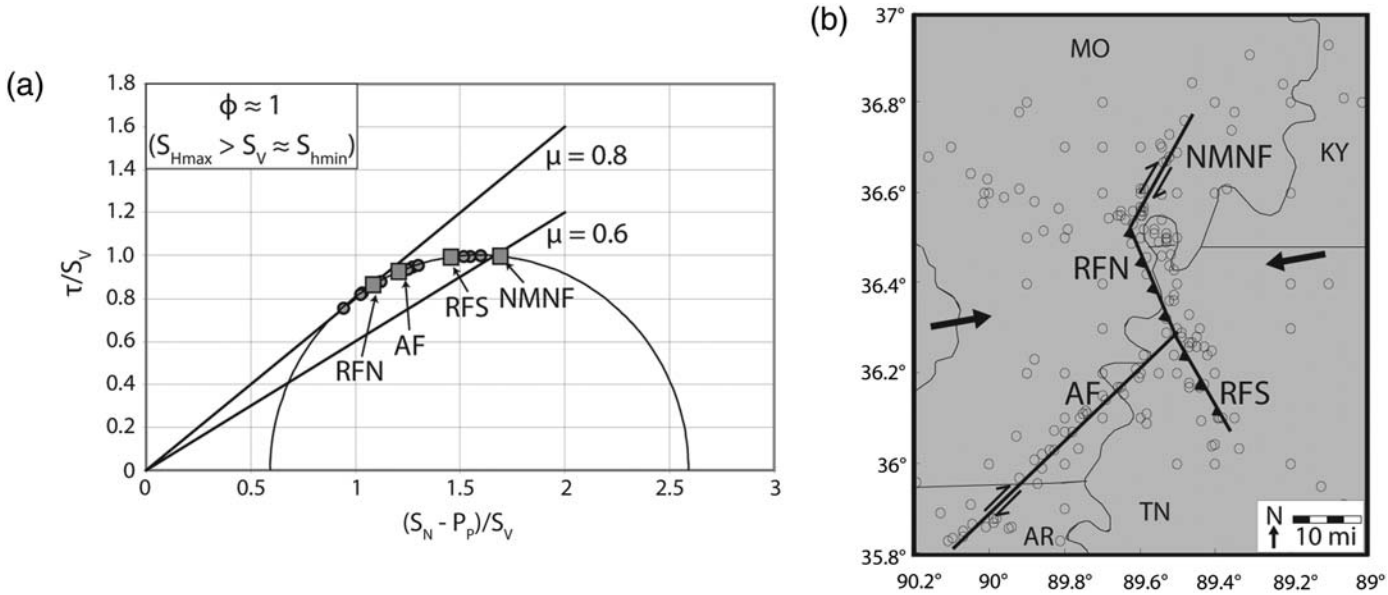

▲ **Figure 4.** (a) Mohr diagram illustrating frictional slip compatibility of preferred focal mechanism nodal planes (circles) and large-scale NMSZ faults (squares) assuming a uniform, transpressional stress field and hydrostatic pore pressure. Note both axes are normalized by the vertical stress (S_V). Ten of the twelve focal mechanisms have at least one nodal plane that is frictionally consistent with slip ($0.6 < \mu < 0.8$). All four large-scale NMSZ fault segments are also frictionally consistent with slip. AF = Axial fault, RFS = Reelfoot fault, southern segment, RFN = Reelfoot fault, northern segment, NMNF = New Madrid north fault. (b) Large-scale NMSZ faults examined for frictional slip compatibility in the local stress field. Analysis results are listed in Table 2. The large, black arrows represent the orientation of $S_{H\max}$ inferred from focal mechanism *P*-axes in this study. Fault trends are modified from Csontos and Van Arsdale (2008).

with $\mu = 0.6$. Note that the conjugate nodal planes have significantly higher misfits of 25° in strike and 14° in dip. For test planes that slip with $\mu = 0.8$, the average misfit from the preferred nodal plane is less than 20° in strike and dip (not shown). Because the preferred nodal plane misfits are within the range of uncertainty associated with the stress measurements and focal mechanism solutions, we conclude that the preferred nodal planes are slip-compatible in the current stress field.

A second approach for testing frictional slip compatibility utilizes a simplified version of the first approach. Instead of calculating relative principal stress magnitudes from each focal mechanism, a uniform stress field where $\Phi \approx 0$ and $S_{H\max}$ is oriented N80°E is prescribed across the entire NMSZ. The Φ value corresponds to a transpressional stress regime where $S_{H\max} > S_V \approx S_{h\min}$. A transpressional stress regime is selected based on the average Φ value of the 12 focal mechanisms (0.38 ± 0.2) and the prevalence of strike-slip and thrust focal mechanisms across the NMSZ. The N80°E $S_{H\max}$ orientation is chosen based on the dominant ENE-WSW $S_{H\max}$ trend within the study area. Assuming the uniform stress field and hydrostatic pore pressure, the Mohr–Coulomb criterion is again used to calculate the friction coefficient required for slip on all focal mechanism nodal planes. Ten of the twelve focal mechanisms have at least one nodal plane that slips with $0.6 < \mu < 0.8$. In other words, the nodal planes slip with friction coefficients consistent with those derived from laboratory experiments (Byerlee, 1978). The frictional slip compatibility is shown graphically on a Mohr diagram normalized by the vertical stress in Figure 4a. The nodal planes are represented by the gray circles. The remaining two focal mechanisms would only require minimal nodal plane rotations (10° in strike, for example) to have one nodal plane become slip compatible ($0.6 < \mu < 0.8$).

A third approach examines the frictional slip compatibility of large-scale fault planes delineated from seismicity clusters within the NMSZ. Four fault planes representing the New Madrid North, Reelfoot (northern and southern segments), and Axial faults are examined (Fig. 4b and Table 2). Using the Mohr–Coulomb criterion with the uniform, transpressional stress field and hydrostatic pore pressure, we find all four fault planes are compatible with slip in the current stress field with $0.58 < \mu < 0.8$ (Table 2). The slip compatibility of each plane is shown on a Mohr diagram in Figure 4a (gray squares).

DISCUSSION

The 12 individual focal mechanism *P*-axes indicate a consistent ENE-WSW maximum horizontal compressive stress across the NMSZ. This represents a 20–30° clockwise rotation from the dominant NE–SW $S_{H\max}$ trend observed throughout most of the eastern United States and southeastern Canada thought to derive from buoyancy-driven forces (ridge push) (Zoback and Zoback, 1980, 1989, 2007). While this minor rotation is similar in scale to the uncertainties in many stress measurements, our careful data selection procedure and the consistency of

$S_{H\max}$ orientations with different types of stress measurements in the NMSZ implies that this is a robust observation. Several studies have suggested that $S_{H\max}$ orientations perturb locally within the NMSZ (O'Connell *et al.*, 1982; Liu, 1997), possibly reflecting complex fault interactions (Russ, 1982). While transient local stress states may exist near major fault intersections, the stress measurements inferred in this study as well as the vast majority of measurements in the WSM database indicate a consistent $S_{H\max}$ orientation throughout the NMSZ.

The slip compatibility results indicate that NMSZ faults are well oriented for shear slip in the contemporary stress field and generally do not require elevated pore pressure, local stress sources, or anomalous fault friction to enable shear failure (they are slip-compatible). The results also compliment the conclusions of Zoback (1992) and Hurd and Zoback (2012) which demonstrated general slip compatibility of intraplate faults in the current stress field using larger focal mechanism data sets spanning the central and eastern United States and eastern Canada. Furthermore, the findings corroborate previous qualitative assessments that the fault patterns and deformation styles inferred from NMSZ focal mechanisms are consistent with an ENE-WSW $S_{H\max}$ orientation (Zoback and Zoback, 1981, 1989). While we acknowledge that fault interactions and igneous intrusions may locally affect stress distributions within the NMSZ (O'Connell *et al.*, 1982; Andrews *et al.*, 1985; Ellis, 1994; Hildenbrand and Hendricks, 1995; Liu, 1997; Hildenbrand *et al.*, 2001), our results quantitatively demonstrate that local stress perturbations are not required to explain slip on most NMSZ faults.

Friction coefficients (μ) between 0.6 and 0.8 are considered in our analysis based on multiple lines of evidence. First, Byerlee (1978) demonstrated from laboratory experiments that μ generally falls between 0.6 and 1.0 for a wide variety of rock types over a range of confining pressures, although it may be lower in shaly rocks, which is not relevant to NMSZ earthquakes. Second, in-situ stress measurements as deep as ~8 km in the upper crust are regularly consistent with predicted stress magnitudes using Coulomb frictional-failure theory with $0.6 \leq \mu \leq 1.0$ (fig. 1 in Townend and Zoback, 2000). Lastly, Sibson and Xie (1998) and Collettini and Sibson (2001) demonstrated using the Coulomb failure criterion that dips of active thrust and normal faults associated with relatively large (**M** >5.5) earthquakes are consistent with fault reactivation assuming $0.6 \leq \mu \leq 0.85$ and principal stresses lying in horizontal and vertical planes.

Exhumed major fault zones often illustrate highly variable physical properties between the host rock, damage zone and fault core. These variable physical properties can affect local stress orientations and magnitudes, which may subsequently influence fracture propagation behavior (Gudmundsson *et al.*, 2010). Our analysis directly examines the potential for variable friction coefficients or local stress perturbations to enable slip on NMSZ faults. In particular, a uniform stress field is applied over the NMSZ, and the friction coefficient required for shear failure is calculated for each fault plane. Even in this homogeneous stress configuration, friction coefficients consistent with empirical observations can explain slip on most NMSZ faults assuming hydrostatic pore pressure in the brittle crust. Thus, the scale of perturbation considered by Gudmundsson *et al.* (2010) (and many others) appears to be smaller than the scale primarily driving large-scale earthquake rupture.

Previous researchers have suggested that NMSZ faulting may be controlled in part by elevated fluid pressures in the upper crust (Al-Shukri and Mitchell, 1988; McKeown and Diehl, 1994; Powell *et al.*, 2010). The hydrostatic pore pressure assumption used in this study is based on widespread observations of hydrostatic pore pressure persisting to as deep as 12 km in the upper crust (table 1 in Townend and Zoback, 2000) and the consistency of hydrostatic pore pressure in the upper crust in maintaining observed lithospheric deformation rates in force-limited stress models (Zoback and Townend, 2001). While active faults can often be conduits for fluid flow, our results and those from Zoback (1992) indicate that it is generally not necessary to prescribe substantially elevated fluid pressure in the intraplate crust to enable fault slip. Moreover, they further support the hypothesis that the brittle crust is generally in a state of frictional failure equilibrium due to regional plate-driving forces (Zoback *et al.*, 2002) with regional variations reflecting changes of lithospheric density (Zoback and Mooney, 2003).

The slip incompatibility of the two original focal mechanisms from Herrmann (1979) and compatibility of the revised mechanisms from Herrmann and Ammon (1997) highlights the importance of having well-constrained stress data. This is particularly significant for focal mechanisms, which are a primary source of stress information in the NMSZ and consequently the basis of many tectonic interpretations. Quality guidelines for stress measurements were presented by Zoback and Zoback (1989), although the inherent subjectivity of the ranking criteria requires that careful examination and selection is always necessary. Newer focal mechanisms constrained by waveform modeling, such as those from the Saint Louis University Earthquake Center, are more reliable and often present much more self-consistent stress information with nearby data points than mechanisms constrained with less stringent techniques. High-resolution seismic monitoring has been in place over the entire NMSZ and Mississippi embayment with the repositioning of EarthScope's U.S. Transportable Array of broadband seismometers over the central U.S. during 2011. This seismic data will hopefully lead to improved hypocenter locations and focal mechanisms, enhanced images of seismogenic fault planes, and improved tectonic models of the NMSZ.

CONCLUSIONS

In this study, we revisited the question of fault slip in the New Madrid seismic zone within the current stress field originally addressed by Zoback (1992). We compiled a set of 12 well-constrained focal mechanisms from earthquakes occurring in the NMSZ and four large-scale NFSZ fault planes delineated from seismicity clusters. Using this data, we updated

the local stress map, examined the consistency of $S_{H\max}$ orientations across the NMSZ, and investigated fault stability. The 12 focal mechanism *P*-axes indicate a consistent ENE-WSW $S_{H\max}$ orientation, which is in agreement with preexisting stress measurements in the World Stress Map database. The ENE-WSW trend represents a slight clockwise rotation from the NE–SW $S_{H\max}$ orientation observed over much of the central and eastern United States.

To examine fault stability, we used the Mohr–Coulomb failure criterion to calculate the friction coefficients required for shear failure on the focal mechanism nodal planes and large-scale fault planes assuming a uniform, transpressional stress field and hydrostatic pore pressure. Nearly all fault planes are compatible with shear slip with laboratory-determined coefficients of friction ($0.6 < \mu < 0.8$) within the uniform stress field. We therefore conclude that, in general, elevated pore pressures, local stress perturbations or anomalous fault strength are not necessary to explain the faulting within the NMSZ. Our conclusions support the findings of Zoback (1992) in the central and eastern United States as well as previous qualitative arguments by Zoback and Zoback (1981, 1989) that NMSZ faults are well-oriented for slip in an ENE-WSW compressive stress field.

ACKNOWLEDGMENTS

Support for Owen Hurd was provided through teaching and research assistantships from the Stanford University Geophysics Department.

REFERENCES

Al-Shukri, H. J., and B. J. Mitchell (1988). Reduced seismic velocities in the source zone of New Madrid earthquakes, *Bull. Seismol. Soc. Am.* **78,** 1491–1509.

Andrews, M. C., W. D. Mooney, and R. P. Meyer (1985). The relocation of microearthquakes in the northern Mississippi embayment, *J. Geophys. Res.* **90,** 10223–10236.

Angelier, J. (1979). Determination of the mean principal directions of stresses for a given fault population, *Tectonophysics* **56,** T17–T26.

Baldwin, J. N., J. B. Harris, R. B. Van Arsdale, R. Givler, K. I. Kelson, J. L. Sexton, and M. Lake (2005). Constraints on the location of the Late Quaternary Reelfoot and New Madrid north faults in the northern New Madrid seismic zone, central United States, *Seismol. Res. Lett.* **76,** 772–789.

Braile, L. W., W. J. Hinze, G. R. Keller, E. G. Lidiak, and J. L. Sexton (1986). Tectonic development of the New Madrid rift complex, Mississippi embayment, North America, *Tectonophysics* **131,** 1–21.

Byerlee, J. D. (1978). Friction of rock, *Pure Appl. Geophys.* **116,** 615–626.

Calais, E., A. M. Freed, R. Van Arsdale, and S. Stein (2010). Triggering of New Madrid seismicity by late-Pleistocene erosion, *Nature* **466,** 608–612.

Chiu, J. M., A. Johnston, and Y. Yang (1992). Imaging the active faults of the central New Madrid seismic zone using PANDA array data, *Seismol. Res. Lett.* **63,** 375–393.

Collettini, C., and R. H. Sibson (2001). Normal faults, normal friction? *Geology* **29,** 927–930.

Csontos, R., and R. Van Arsdale (2008). New Madrid seismic zone fault geometry, *Geosphere* **4,** 802–813.

Dart, R. L., and H. S. Swolfs (1998). Contour mapping of relic structures in the Precambrian basement of the Reelfoot rift, North American midcontinent, *Tectonics* **17,** 235–249.

Dunn, M., S. Horton, H. DeShon, and C. Powell (2010). High-resolution earthquake relocation in the New Madrid Seismic Zone, *Seismol. Res. Lett.* **81,** 406–413.

Ellis, W. L. (1994). Summary and discussion of crustal stress data in the region of the New Madrid seismic zone, *U.S. Geol. Surv. Profess. Pap. 1538A-C*, B1–B13.

Ervin, C. P., and L. D. McGinnis (1975). Reelfoot rift: Reactivated precursor to the Mississippi embayment, *Bull. Seismol. Soc. Am.* **86,** 1287–1295.

Gephart, J. W. (1985). Principal stress directions and the ambiguity in fault plane identification from focal mechanisms, *Bull. Seismol. Soc. Am.* **75,** 621–625.

Grollimund, B., and M. D. Zoback (2001). Did deglaciation trigger intraplate seismicity in the New Madrid seismic zone? *Geology* **29,** 175–178.

Gudmundsson, A., T. H. Simmenes, B. Larsen, and S. L. Philipp (2010). Effects of internal structure and local stresses on fracture propagation, deflection, and arrest in fault zones, *J. Struct. Geol.* **32,** 1643–1655.

Heidbach, O., M. Tingay, A. Barth, J. Reinecker, D. Kurfeß, and B. Müller (2008). The world stress map database release 2008, http://www.world-stress-map.org (last accessed August 2010).

Herrmann, R. B. (1979). Surface wave focal mechanisms for eastern North American earthquakes with tectonic implications, *J. Geophys. Res.* **84,** 3543–3552.

Herrmann, R. B., and C. J. Ammon (1997). Faulting parameters of earthquakes in the New Madrid, Missouri, region, *Eng. Geol.* **46,** 299–311.

Hildenbrand, T. G., and J. D. Hendricks (1995). Geophysical setting of the Reelfoot rift and relations between rift structures and the New Madrid seismic zone, *U.S. Geol. Surv. Profess. Pap. 1528-E*, 30 pp.

Hildenbrand, T. G., W. D. Stuart, and P. Talwani (2001). Geologic structures related to New Madrid earthquakes near Memphis, Tennessee, based on gravity and magnetic interpretations, *Eng. Geol.* **62,** 105–121.

Himes, L., W. Stauder, and R. B. Herrmann (1988). Indication of active faults in the New Madrid seismic zone from precise location of hypocenters, *Seismol. Res. Lett.* **59,** 123–131.

Hurd, O., and M. D. Zoback (2012). Intraplate earthquakes, regional stress and fault mechanics in the central and eastern U.S. and southeastern Canada, *Tectonophysics* (in press).

Jaeger, J. C., and N. G. W. Cook (1979). *Fundamentals of Rock Mechanics*, Chapman and Hall, London, 475 pp.

Johnston, A. C., and E. S. Schweig (1996). The enigma of the New Madrid earthquakes of 1811–1812, *Annu. Rev. Earth Planet. Sci.* **24,** 339–384.

Lay, T., and T. C. Wallace (1995). *Modern Global Seismology*, Academic Press, San Diego, 397–433.

Lamont-Doherty Cooperative Seismograph Network, http://www.ldeo.columbia.edu/LCSN/ (last accessed August 2011).

Liu, Z. (1997). Earthquake modeling and active faulting in the New Madrid seismic zone, *Ph.D. Dissertation*, Saint Louis University.

Mazzotti, S., and J. Townend (2010). State of stress in central and eastern North American seismic zones, *Lithosphere* **2,** 76–83.

McKenzie, D. P. (1969). The relation between fault plane solutions for earthquakes and the directions of the principal stresses, *Bull. Seismol. Soc. Am.* **59,** 591–601.

McKeown, F. A., and S. F. Diehl (1994). Evidence of contemporary and ancient excess fluid pressure in the New Madrid seismic zone of the Reelfoot Rift, central United States, in *Investigations of the*

New Madrid Seismic Zone, K. M. Shedlock and A. C. Johnston (Editors), *U.S. Geol. Surv. Profess. Pap. 1538-N*, 24 pp.

Mueller, K., and J. Pujol (2001). Three-dimensional geometry of the Reelfoot blind thrust: Implications for moment release and earthquake magnitude in the New Madrid seismic zone, *Bull. Seismol. Soc. Am.* **91,** 1563–1573.

Nuttli, O. W. (1973). The Mississippi Valley earthquakes of 1811–1812: Intensities, ground motion and magnitudes, *Bull. Seismol. Soc. Am.* **63,** 227–248.

O'Connell, D. R., C. G. Bufe, and M. D. Zoback (1982). Microearthquakes and faulting in the area of New Madrid, Missouri-Reelfoot Lake, Tennessee, in *Investigations of the New Madrid, Missouri, Earthquake Region*, F. A. McKeown and L. C. Pakiser (Editors), *U.S. Geol. Surv. Profess. Pap. 1236*, 31–38.

Powell, C. A., M. M. Withers, H. R. DeShon, and M. M. Dunn (2010). Intrusions and anomalous V_P/V_S ratios associated with the New Madrid seismic zone, *J. Geophys. Res.* **115,** B08311.

Pratt, T. L. (1994). How old is the New Madrid seismic zone? *Seismol. Res. Lett.* **65,** 172–179.

Pujol, J., A. Johnston, J.-M. Chiu, and Y.-T. Yang (1997). Refinement of thrust faulting models for the central New Madrid seismic zone, *Eng. Geol.* **46,** 281–298.

Russ, D. P. (1982). Style and significance of surface deformation in the vicinity of New Madrid, Missouri, in *Investigations of the New Madrid, Missouri, Earthquake Region*, F. A. McKeown and L. C. Pakiser (Editors), *U.S. Geol. Surv. Profess. Pap.* **1236,** 95–114.

Saint Louis University Earthquake Center. http://www.eas.slu.edu/Earthquake_Center/MECH.NA/index.html (last accessed July 2011).

Schweig, E. S., and M. A. Ellis (1994). Reconciling short recurrence intervals with minor deformation in the New Madrid seismic zone, *Science* **264,** 1308–1311.

Sibson, R. H., and G. Xie (1998). Dip range for intracontinental reverse fault ruptures: Truth not stranger than friction? *Bull. Seismol. Soc. Am.* **88,** 1014–1022.

Stauder, W., M. Kramer, G. Fischer, S. Schaefer, and S. T. Morrissey (1976). Seismic characteristics of southeast Missouri as indicated by a regional telemetered micro-earthquake array, *Bull. Seismol. Soc. Am.* **66,** 1953–1964.

Townend, J., and M. D. Zoback (2000). How faulting keeps the crust strong, *Geology* **28,** 399–402.

Tuttle, M. P., E. S. Schweig III, J. Campbell, P. M. Thomas, J. D. Sims, and R. H. Lafferty III (2005). Evidence for New Madrid earthquakes in A.D. 300 and 2350 B.C., *Seismol. Res. Lett.* **76,** 489–501.

Van Arsdale, R. (2000). Displacement history and slip rate on the Reelfoot fault of the New Madrid seismic zone, *Eng. Geol.* **55,** 219–226.

Zoback, M. D., R. M. Hamilton, A. J. Crone, D. P. Russ, F. A. McKeown, and S. R. Brockman (1980). Recurrent intraplate tectonism in the New Madrid seismic zone, *Science* **209,** 971–976.

Zoback, M. D., and J. Townend (2001). Implications of hydrostatic pore pressures and high crustal strength for the deformation of intraplate lithosphere, *Tectonophysics* **336,** 19–30.

Zoback, M. D., J. Townend, and B. Grollimund (2002). Steady-state failure equilibrium and deformation of intraplate lithosphere, *Int. Geol. Rev.* **44,** 383–401.

Zoback, M. D., and M. L. Zoback (1981). State of stress and intraplate earthquakes in the United States, *Science* **213,** 96–104.

Zoback, M. L. (1992). Stress field constraints on intraplate seismicity in eastern North America, *J. Geophys. Res.* **97,** 11761–11782.

Zoback, M. L., and W. D. Mooney (2003). Lithospheric buoyancy and continental intraplate stress, *Int. Geol. Rev.* **45,** 95–118.

Zoback, M. L., and M. D. Zoback (1980). State of stress of the conterminous United States, *J. Geophys. Res.* **85,** 6113–6156.

Zoback, M. L., and M. D. Zoback (1989). Tectonic stress field of the conterminous United States, *Mem. Geol. Soc. Am.* **172,** 523–539.

Zoback, M. L., and M. D. Zoback (2007). Lithosphere Stress and Deformation, in *Earthquake Seismology—Treatise on Geophysics*, Vol. **6**, A. Watts and G. Schubert (Editors), Elsevier Ltd., Amsterdam, 253–274.

Owen Hurd
Mark D. Zoback
Department of Geophysics
Stanford University
397 Panama Mall
Stanford, California 94305-2215 U.S.A.
ohurd@stanford.edu